Electronic Supplementary Material (ESI) for Dalton Transactions.

Supporting Information

A multifunctional anionic metal-organic framework for high proton-conductivity and photoreduction of CO_2 induced by cation exchange

Hong-Xu Sun,[a] Hai-Ning Wang,[a] Yao-Mei Fu,[b] Xing Meng,*[a] Yu-Ou He,[a] Rui-Gang Yang,[a] Zhen Zhou[a] and Zhong-Min Su[b,c]

[a]School of Chemistry and Chemical Engineering, Shandong University of Technology, Zibo, 255049, China. E-mail: *mengxing837@foxmail.com*.

[b]Shandong Engineering Research Center of Green and High-value Marine Fine Chemical; Weifang University of Science and Technology, Shouguang, 262700, China

[c]School of Chemistry and Environmental Engineering, Changchun University of Science and Technology, Changchun, 130022, China

E-mail: mengxing837@foxmail.com

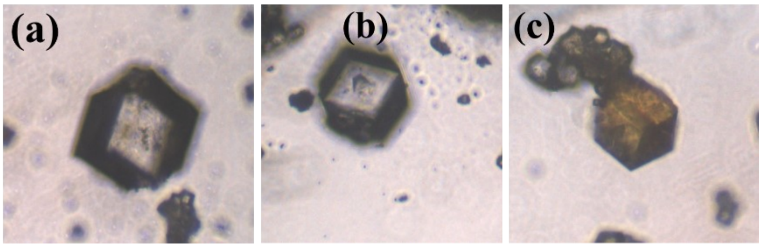

Fig. S1 Optical micrograph of **In-MOF24** (a), **NH_4^+@In-MOF24** (b) and **Rubpy@In-MOF24-15** (c).

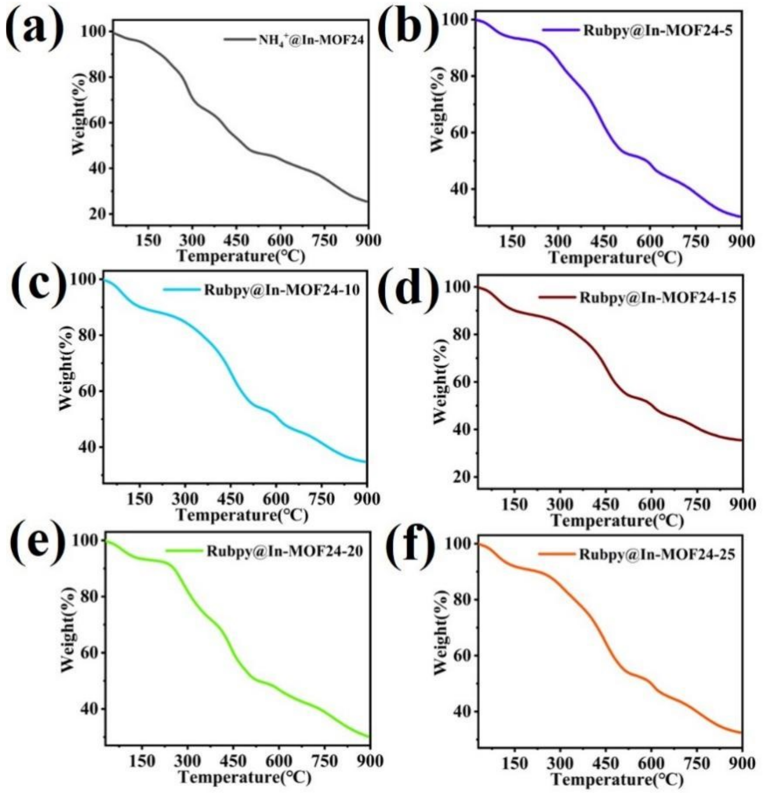

Fig. S2 TG curve of **NH_4^+@In-MOF24** (a), **Rubpy@In-MOF24-5** (b), **Rubpy@In-MOF24-10** (c), **Rubpy@In-MOF24-15** (d), **Rubpy@In-MOF24-20** (e) and **Rubpy@In-MOF24-25** (f).

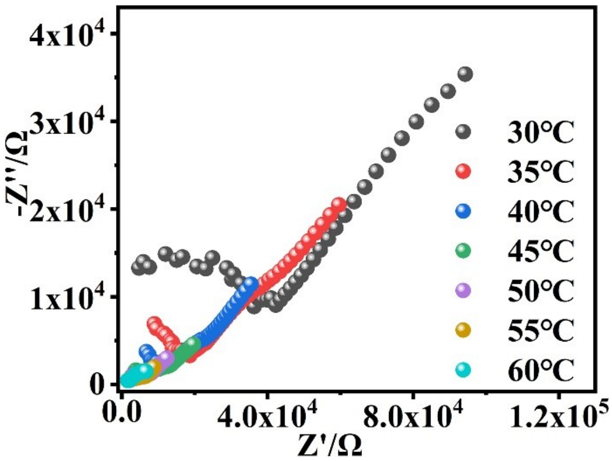

Fig. S3 Impedance spectra of **In-MOF24** at 95%RH with different temperatures.

Table S1 Proton conductivities of **In-MOF24** at 95%RH under different temperatures.

Temperature (°C)	**In-MOF24** (S cm^{-1})
30	4.28×10^{-7}
35	1.62×10^{-6}
40	3.67×10^{-6}
45	9.44×10^{-6}
50	2.05×10^{-5}

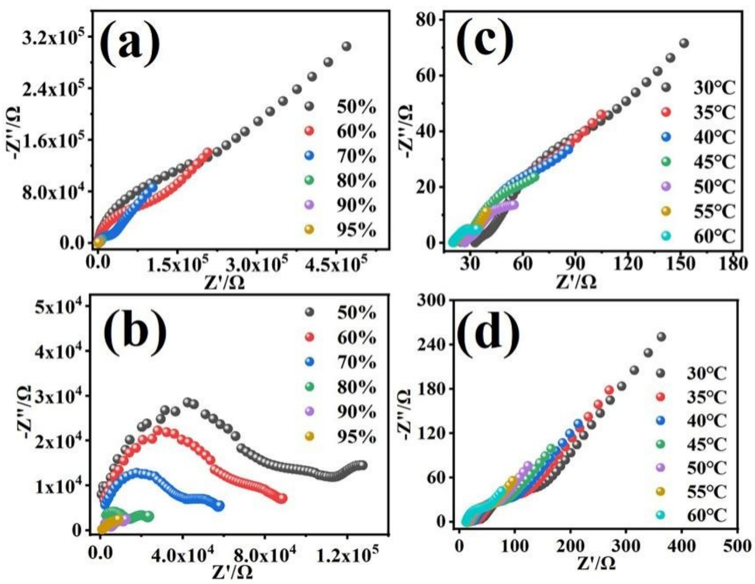

Fig. S4 Impedance spectra of **NH_4^+@In-MOF24** (a) and **Li^+@In-MOF24** (b) at 30°C with different RHs, and **NH_4^+@In-MOF24** (c) and **Li^+@In-MOF24** (d) at 95%RH with different temperatures.

Table S2 Proton conductivities of **NH_4^+@In-MOF24** and **Li^+@In-MOF24** at 30°C under different relative humidity.

Humidity (% RH)	**NH_4^+@In-MOF24** (S cm^{-1})	**Li^+@In-MOF24** (S cm^{-1})
50	4.27×10^{-7}	6.58×10^{-7}
60	8.86×10^{-7}	9.17×10^{-7}
70	4.34×10^{-6}	1.47×10^{-6}
80	3.19×10^{-5}	4.11×10^{-6}
90	1.41×10^{-4}	7.65×10^{-6}
95	6.93×10^{-4}	3.32×10^{-4}

Table S3 Proton conductivities of **NH_4^+@In-MOF24** and **Li^+@In-MOF24** at 95%RH under different temperatures.

Temperature (°C)	**NH_4^+@In-MOF24** (S cm^{-1})	**Li^+@In-MOF24** (S cm^{-1})
30	6.93×10^{-4}	3.32×10^{-4}
35	1.05×10^{-3}	4.06×10^{-4}
40	1.35×10^{-3}	4.69×10^{-4}
45	2.44×10^{-3}	5.30×10^{-4}
50	3.64×10^{-3}	7.07×10^{-4}
55	5.39×10^{-3}	8.02×10^{-4}
60	9.81×10^{-3}	8.72×10^{-4}

Table S4 Proton conductive MOFs and their proton conductivity.

Materials	**Proton conductivity (S cm^{-1})**	**Condition**	**Refs**
CDs@MOF-802	1.13×10^{-1} S·cm^{-1}	25°C, 98% RH	1
Im@MOF-808	3.45×10^{-2} S·cm^{-1}	60 °C, 99% RH	2
$Gd_2(H_3nmp)_2]\cdot xH_2O$	3.97×10^{-2} S·cm^{-1}	94°C, 98% RH	3
NH_4^+@In-MOF24	**9.81×10^{-3} S·cm^{-1}**	**60°C, 95% RH**	**This work**
$\{Na[Cd(MIDC)]\}_n$	1.04×10^{-3} S·cm^{-1}	100°C, 98% RH	4
$[Cu_2(DHBDI)_3(SO_4)_2]n$	1.14×10^{-3} S·cm^{-1}	90°C, 98% RH	5
Cd-MOF	1.15×10^{-3} S·cm^{-1}	90°C, 98% RH	6
MOF-801	1.88×10^{-3} S·cm^{-1}	25°C, 98% RH	7
Eu(iii)-MOF	3.5×10^{-3} S·cm^{-1}	80°C, 98% RH	8
$(H[Ln(H_2O)_4]_2[MnV_{13}O_{38}]\cdot 9NMP\cdot 17 H_2O$ (Ln=Ce and La)	$4.68/3.46\times10^{-3}$ S·cm^{-1}	61°C, 97% RH	9
UiO-66-N_3	8.8×10^{-3} S·cm^{-1}	80°C, 98% RH	10
MOF-bpy	1.03×10^{-4} S·cm^{-1}	60°C, 93% RH	11
MOF-Eu	1.89×10^{-4} S·cm^{-1}	60°C, 98% RH	12
$[CH_3NH_3]2[H_3O]Ag_5Sn_4Se_{12}\cdot C_2H_5OH$	2.62×10^{-4} S·cm^{-1}	60 °C, 99% RH	13
ZZU-2	4.63×10^{-4} S·cm^{-1}	98 °C, 100% RH	14
Zn-SDC-MOF	8×10^{-4} S·cm^{-1}	25°C, 95% RH	15

MFM-510	2.1×10^{-5} S·cm^{-1}	25°C, 99% RH	16

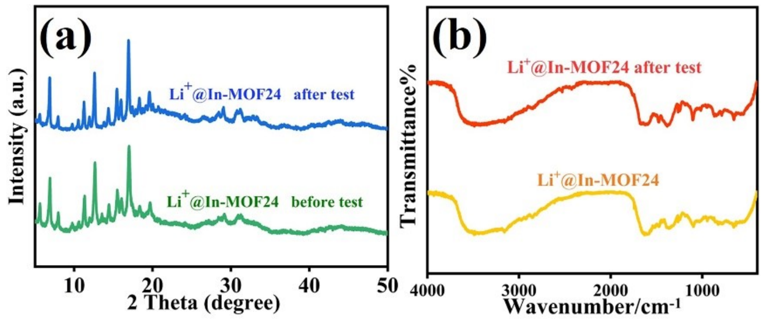

Fig. S5 The PXRD patterns of the **Li$^+$@In-MOF24** before test and after test (a) and the FT-IR spectra of **Li$^+$@In-MOF24** before test and after test (b).

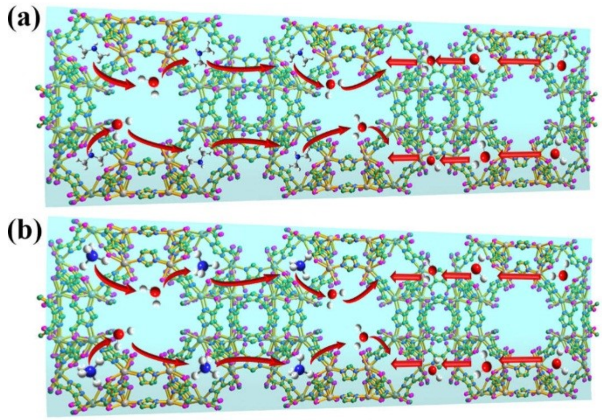

Fig. S6 The proton conduction pathway of **In-MOF24** (a) and **NH$_4^+$@In-MOF24** (b).

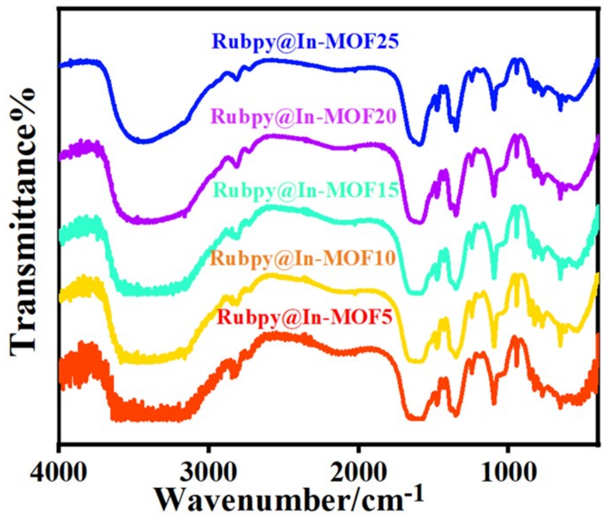

Fig. S7 FT-IR spectra of **Rubpy@In-MOF24-5**, **Rubpy@In-MOF24-10**, **Rubpy@In-MOF24-15**, **Rubpy@In-MOF24-20** and **Rubpy@In-MOF24-25**.

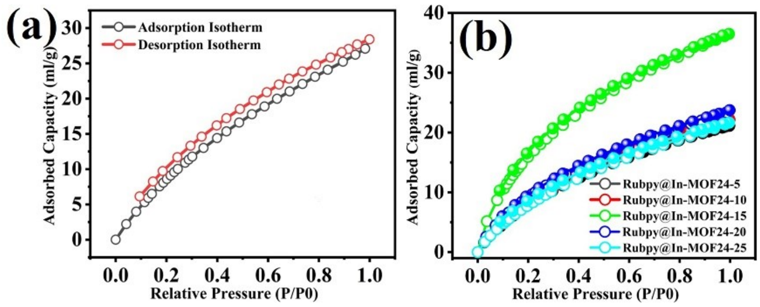

Fig. S8 CO_2 adsorption-desorption isotherms of **In-MOF24** (a) and **Rubpy@In-MOF24-5**, **Rubpy@In-MOF24-10**, **Rubpy@In-MOF24-15**, **Rubpy@In-MOF24-20** and **Rubpy@In-MOF24-25** at 273K (b).

Table S5 The Brunauer-Emmett-Teller (BET) specific surface areas of **In-MOF24**, **Rubpy@In-MOF24-5**, **Rubpy@In-MOF24-10**, **Rubpy@In-MOF24-15**, **Rubpy@In-MOF24-20** and **Rubpy@In-MOF24-25**.

Material	CO_2 sorption (ml/g)
In-MOF24	28.41
Rubpy@In-MOF24-5	21.12
Rubpy@In-MOF24-10	22.16
Rubpy@In-MOF24-15	36.49
Rubpy@In-MOF24-20	23.73
Rubpy@In-MOF24-25	21.65

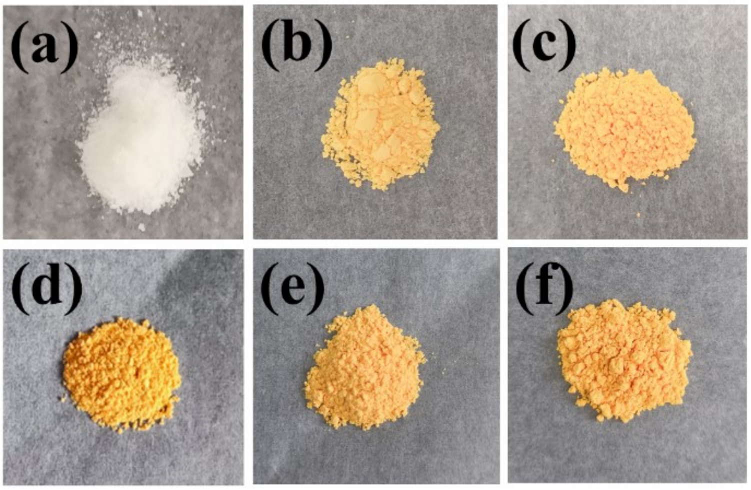

Fig. S9 Optical picture of **In-MOF24** (a), **Rubpy@In-MOF24-5** (b), **Rubpy@In-MOF24-10** (c), **Rubpy@In-MOF24-15** (d), **Rubpy@In-MOF24-20** (e) and **Rubpy@In-MOF24-25** (f).

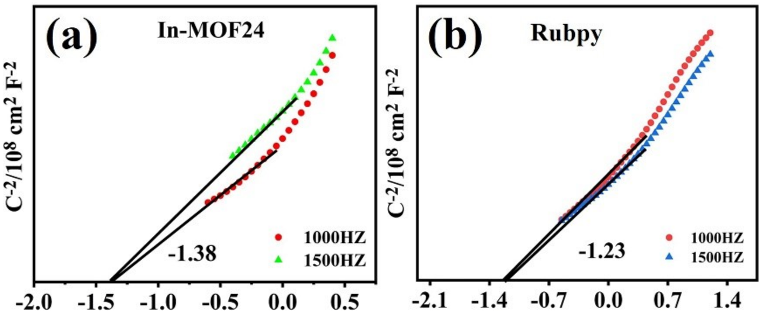

Fig. S10 Mott-Schottky plots of **In-MOF24** (a) and Rubpy (b).

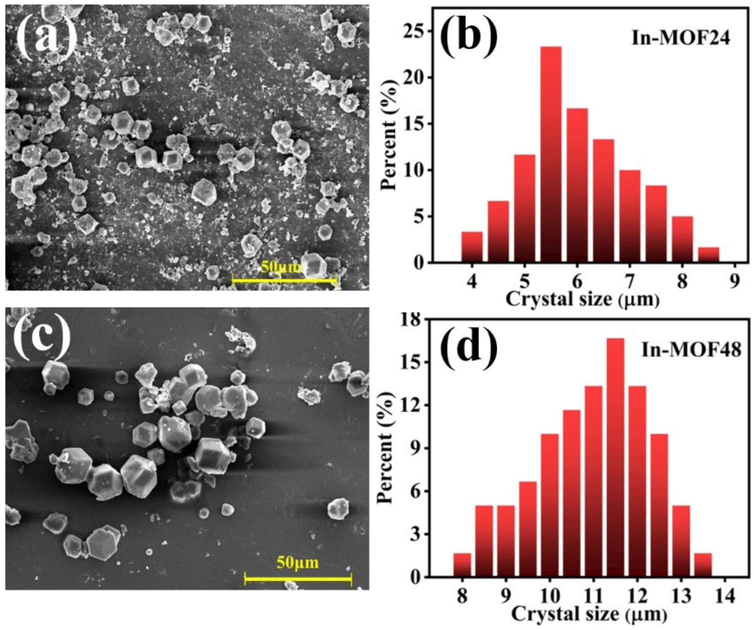

Fig. S11 SEM image of **In-MOF24** (a) and **In-MOF48** (c), crystal size distribution map of **In-MOF24** (b) and **In-MOF48** (d).

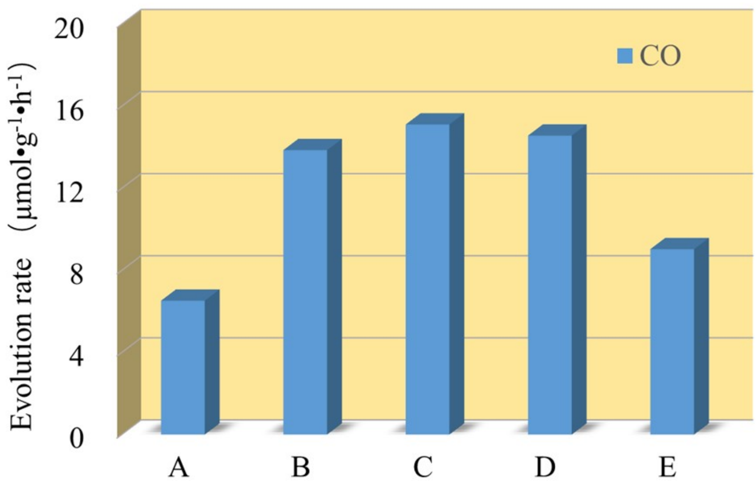

Fig. S12 The efficiencies of **Rubpy@In-MOF24-5** (A), **Rubpy@In-MOF24-10** (B), **Rubpy@In-MOF24-15** (C), **Rubpy@In-MOF24-20** (D) and **Rubpy@In-MOF24-25** (E) on the evolution of CO_2 irradiated with visible light for 2h under 10% CO_2

conditions.

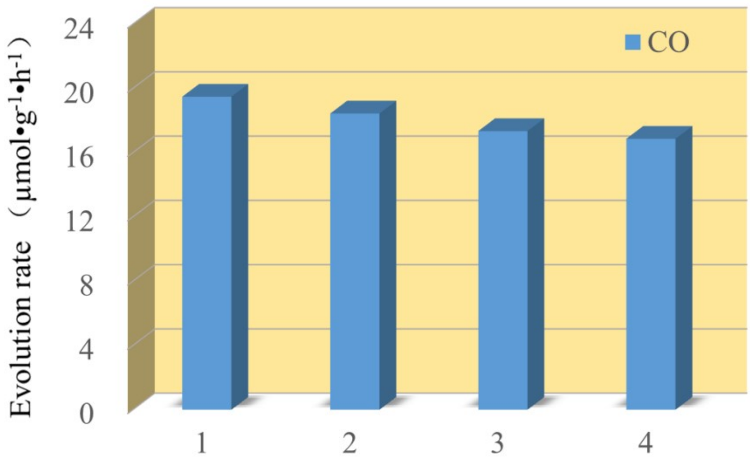

Fig. S13 The photocatalytic recyclability of **Rubpy@In-MOF24-15**.

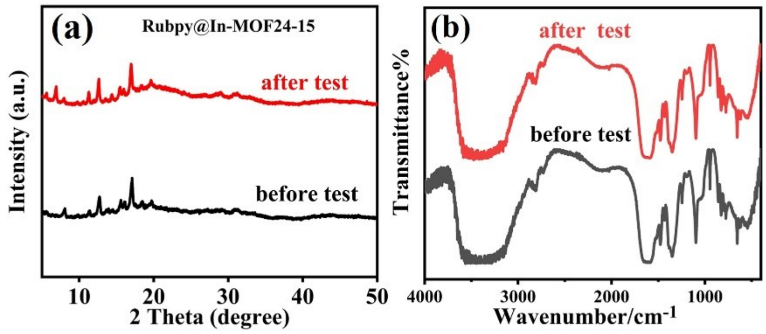

Fig. S14 The PXRD patterns of the **Rubpy@In-MOF24-15** before test and after test (a) and the FT-IR spectra of **Rubpy@In-MOF24-15** before test and after test (b).

Table S6 The photocatalytic performances of MOFs with H_2O as sacrificial reagents.

Materials	Products	Formation rate	Reaction agent	Refs
Rubpy@In-MOF24-15	**CO**	**18.51 μmol g^{-1} h^{-1}**	**H_2O**	**This work**
MOF-Ni	CO	371.6 μmol g^{-1} h^{-1}	H_2O	18
Mn-MOF	CO	21 μmol g^{-1} h^{-1}	H_2O	19
UiO-66	CO	1.0 μmol g^{-1} h^{-1}	H_2O	20
TiO_2/ZIF-8-G2	CO	21.74 μmol g^{-1} h^{-1}	H_2O	21
NNU-31-Zn	HCOOH	26.3 μmol g^{-1} h^{-1}	H_2O	22
$CsPbBr_3$@ZIF-67	CH_4	29.63 μmol g^{-1} h^{-1}	H_2O	23
$Cu_3(BTC)_2$@TiO_2	CH_4	2.64 μmol g^{-1} h^{-1}	H_2O	24
TiO_2/Co-ZIF-9	CO	17.58 μmol g^{-1} h^{-1}	H_2O	25

Bi_2S_3/UiO-66	CO	25.6 μmol g^{-1} h^{-1}	H_2O	26
Au@NENU-10	CO	12.8 μmol g^{-1} h^{-1}	H_2O	27
QS-Co_3O_4(ZIF-67)	CO	46.3 μmol g^{-1} h^{-1}	H_2O	28
$CsPbBr_3$QDs/UiO-66(NH_2)	CO	8.21 μmol g^{-1} h^{-1}	H_2O	29
TiO_2/CPO-27-Mg	CO	4.09 μmol g^{-1} h^{-1}	H_2O	30

Notes and references

1. J. Zhang, R. Zhang, Y. Y. Liu, Y. R. Kong, H. B. Luo, Y. Zou, L. Zhai and X. M. Ren, Acidic Groups Functionalized Carbon Dots Capping Channels of a Proton Conductive Metal-Organic Framework by Coordination Bonds to Improve the Water-Retention Capacity and Boost Proton Conduction, *ACS Appl. Mater. Interfaces*., 2021, **13**, 60084-60091.
2. H. B. Luo, Q. Ren, P. Wang, J. Zhang, L. F. Wang and X. M. Ren, High Proton Conductivity Achieved by Encapsulation of Imidazole Molecules into Proton-Conducting MOF-808, *ACS Appl. Mater. Interfaces*., 2019, **11**, 9164-9171.
3. R. F. Mendes, P. Barbosa, E. M. Domingues, P. Silva, F. Figueiredo and F. A. A. Paz Chem, Enhanced proton conductivity in a layered coordination polymer, *Chem. Sci*., 2020, **11**, 6305-6311.
4. R. L. Liu, Y. R. Liu, S. H. Yu, C. L. Yang, Z. F. Li and G. Li, A Highly Proton-Conductive 3D Ionic Cadmium-Organic Framework for Ammonia and Amines Impedance Sensing, *ACS Appl. Mat. Interfaces*., 2019, **11**, 1713-1722.
5. F. Q. Mi, F. X. Ma, S. X. Zou, D. S. Zhan and T. Zhang, A proton-conductive metal-organic framework based on imidazole and sulphate ligands, *Dalton Trans*., 2022, **51**, 1313-1317.
6. F. D. Wang, W. H. Su, C. X. Zhang and Q. L. Wang, High Proton Conductivity of a Cadmium Metal-Organic Framework Constructed from Pyrazolecarboxylate and Its Hybrid Membrane, *Inorg. Chem*., 2021, **60**, 16337-16345.
7. J. Zhang, H. J. Bai, Q. Ren, H. B. Luo, X. M. Ren, Z. F. Tian and S. F. Lu, Extra Water- and Acid-Stable MOF-801 with High Proton Conductivity and Its Composite Membrane for Proton Exchange Membrane, *ACS Appl. Mater. Interfaces*., 2018, **10**, 28656-28663.
8. L. Feng, T. Y. Zeng, H. B. Hou, H. Zhou and J. Tian, Theoretical hydrogen bonding calculations and proton conduction for Eu(iii)-based metal-organic framework, *RSC Adv*., 2021, **11**, 11495-11499.
9. J. X. Wang, Y. D. Wang, M. J. Wei, H. Q. Tan, Y. H. Wang, H. Y. Zang and Y. G. Li, Inorganic open framework based on lanthanide ions and polyoxometalates with high proton conductivity, *Inorg. Chem. Front*., 2018, **5**, 1213-1217.
10. X. N. Zou, D. S. Zhang, Y. L. Xie, T. X. Luan, W. C. Li, L. Li and P. Z. Li, High Enhancement in Proton Conductivity by Incorporating Sulfonic Acids into a

Zirconium-Based Metal-Organic Framework via "Click" Reaction, *Inorg. Chem.*, 2021, **60**, 10089-10094.
11. H. F. Wang, T. Y. Wen, Z. C. Shao, Y. J. Zhao, Y. Cui, K. Gao, W. J. Xu and H. W. Hou, High Proton Conductivity in Nafion/Ni-MOF Composite Membranes Promoted by Ligand Exchange under Ambient Conditions, *Inorg. Chem.*, 2021, **60**, 14, 10492–10501.
12. F. M. Wang, B. X. Hu, W. P. Lustig, L. Zhou, J. Xiang, L. Z. Chen and J. Li, Three Robust Blue-Emitting Anionic Metal–Organic Frameworks with High Stability and Good Proton Conductivities, *Inorg. Chem.*, 2021, **60**, 17926–17932.
13. H. B. Luo, Q. Ren, Y. Liu, Proton Conduction of an Acid-Resistant Open-Framework Chalcogenidometalate Hybrid in Anhydrous versus Humid Environments, *Inorg. Chem.*, 2020, **59**, 7283-7289.
14. R. L. Liu, W. T. Qu, B. H. Dou, Proton-Conductive 3D LnIII Metal-Organic Frameworks for Formic Acid Impedance Sensing, *Chem Asian J.*, 2020, **15**, 182-190.
15. Y. Son, P. C. Rao, J. Kim, G. Park and M. Yoon, Study of Stability and Proton Conductivity of Zn-based Metal-Organic Framework, *B Kor Chem Soc.*, 2021, **42**, 810-817.
16. P. Rought, C. Marsh, O. logo, S. Pili, V. G. Sakai, M. Li, M. S. Brown, S. P. Argent, I. V. Yrezabal, G. Whitehead, M. R. Warren, S. Yang and M. Schröder, Modulating proton diffusion and conductivity in metal-organic frameworks by incorporation of accessible free carboxylic acid groups, *Chem. Sci.*, 2019, **10**, 1492-1499.
17. S. M. Lia, F. Wu, R. B. Lin, J. Wang, C. X. Li, Z. Q. Li, J. Jiang and Y. J. Xiong, Enabling photocatalytic hydrogen production over Fe-based MOFs by refining band structure with dye sensitization, *Chem Eng J.*, 2022, **429**, 132217.
18. X. K. Wang, j. liu, L. Zhang, L. Z. Dong, S. L. Li, Y. H. Kan, D. S. Li, and Y. Q. Lan, Monometallic Catalytic Models Hosted in Stable Metal Organic Frameworks for Tunable CO_2 Photoreduction, *ACS Catal.*, 2019, **9**, 1726-1732.
19. J. H. Qin, P. Xu, Y. D. Huang, L. Y. Xiao, W. W. Lu, X. G. Yang, L. F. Ma and S. Q. Zang, High loading of Mn(II)-metalated porphyrin in a MOF for photocatalytic CO_2 reduction in gas-solid conditions, *Chem. Commun.*, 2021, **57**, 8468-8471.
20. Y. J. Ma, Q. Tang, W. Y. Sun, Z. Y. Yao, W. H. Zhu, T. Li, J. Y. Wang, Assembling ultrafine TiO_2 nanoparticles on UiO-66 octahedrons to promote selective photocatalytic conversion of CO_2 to CH_4 at a low concentration, *Appl. Catal. B-Environ.*, 2020, **270**, 118856-118891.
21. Y. H. Zou, H. N. Wang, X. Meng, H. X. Sun and Z. Y. Zhou, Self-assembly of TiO_2/ZIF-8 nanocomposites for varied photocatalytic CO_2 reduction with H_2O vapor induced by different synthetic methods, *Nanoscale Adv.,* 2021, **3**, 1455-1463.
22. L. Z. Dong, L. Zhang, J. Liu, Q. Huang, M. Lu, W. X. Ji and Y. Q. Lan, Stable Heterometallic Cluster-Based Organic Framework Catalysts for Artificial Photosynthesis, *Angew. Chem. Int. Ed.*, 2020, **59**, 2659-2663.

23. S. Wan, M. Ou, Q. Zhong, X. Wang, Perovskite-type $CsPbBr_3$ quantum dots/UiO-66(NH_2) nanojunction as efficient visible-light-driven photocatalyst for CO_2 reduction, *Chem. Eng. J.*, 2019, **358**, 1287-1295.
24. C. Zheng, X. Y. Qiu, J. Y. Han, Y. F. Wu, S. Q. Liu, Zero-Dimensional-g-CNQD-Coordinated Two-Dimensional Porphyrin MOF Hybrids for Boosting Photocatalytic CO_2 Reduction, *ACS Appl. Mater. Interfaces.*, 2019, **11**, 42243-42249.
25. S. Yan, S. Ouyang, H. Xu, M. Zhao, X. Zhang, J. Ye, Co-ZIF-9/TiO_2 nanostructure for superior CO_2 photoreduction activity, *J. Mater. Chem. A*., 2016, **4**, 15126-15133.
26. X. Chen, Q. Li, J. Li, J. Chen, H. Jia, Modulating charge separation via in situ hydrothermal assembly of low content Bi_2S_3 into UiO-66 for efficient photothermocatalytic CO_2 reduction, *Appl. Catal. B*., 2020, **270**, 118915.
27. S. M. Liu, Z. Zhang, X. Li, H. Jia, M. Ren, S. Liu, Ti-Substituted Keggin-Type Polyoxotungstate as Proton and Electron Reservoir Encaged into Metal-Organic Framework for Carbon Dioxide Photoreduction, *Adv. Mater. Interfaces*., 2018, **5**, 1801062.
28. L. Wang, J. Wan, Y. Zhao, N. Yang, D. Wang, Hollow Multi-Shelled Structures of Co_3O_4 Dodecahedron with Unique Crystal Orientation for Enhanced Photocatalytic CO_2 Reduction, *J. Am. Chem. Soc*., 2019, **141**, 2238-2241.
29. S. Wan, M. Ou, Q. Zhong, X. Wang, Perovskite-type $CsPbBr_3$ quantum dots/UiO-66(NH_2) nanojunction as efficient visible-light-driven photocatalyst for CO_2 reduction, *Chem. Eng. J.*, 2019, **358**, 1287-1295.
30. M. Wang, D. Wang, Z. Li, Self-assembly of CPO-27-Mg/TiO_2 nanocomposite with enhanced performance for photocatalytic CO_2 reduction, *Appl. Catal. B*., 2016, **183**, 47-52.